Copper Systematics in Arc Magmas and Implications for Crust-Mantle Differentiation

Cin-Ty A. Lee *et al.*

Science **336**, 64 (2012);
DOI: 10.1126/science.1217313

Single-particle growth trajectories in the one previous lower-resolution study of Pt nanocrystal growth showed an apparent size decrease after coalescence, as well as a short pause after coalescence before apparent growth by monomer attachment has resumed (fig. S4) (*7*). In the GLC, it is possible to examine and understand in much more detail these unexpected phenomena that follow nanoparticle coalescence. Figure 3C is a plot of the change in length (*l*, along the center-to-center direction), thickness (*t*, vertical direction to the length), and neck diameter (*n*) of the coalesced nanocrystals, whereas Fig. 3D shows the corresponding TEM images. The nanocrystals are connected by a neck at the initial stage of coalescence. Neck growth is accompanied by a decrease in *l* and *t*, which indicates that the atoms migrate to the neck region, presumably by surface diffusion (*31*). After coalescence, the nanocrystal structure also gradually reorganizes, evolving truncated surfaces. Returning to Fig. 2C, the nanocrystal shape after coalescence changes from quasi-spherical to a hexagonal shape that minimizes the surface energy of the nanocrystal as expected from a Wulff construction, also by surface-diffusion processes.

We introduce the GLC as a new type of liquid cell advancing the imaging of liquid-phase systems; encapsulated liquid specimens are observed with an electron microscope at the highest resolution possible to date with minimal sample perturbation. The GLC has enabled the study of colloidal nanocrystal growth with unprecedented resolution, revealing a host of previously unexpected phenomena. We have directly observed the steps of nanocrystal coalescence and oriented attachment at an atomic level. The GLC can be readily applied to directly study a diversity of fluid-phase samples, which beg detailed observation.

References and Notes

1. J. C. Meyer, C. O. Girit, M. F. Crommie, A. Zettl, *Nature* **454**, 319 (2008).
2. C.-Y. Wen *et al.*, *Science* **326**, 1247 (2009).
3. V. Radmilovic *et al.*, *Nat. Mater.* **10**, 710 (2011).
4. A. H. Zewail, *Science* **328**, 187 (2010).
5. N. de Jonge, F. M. Ross, *Nat. Nanotechnol.* **6**, 695 (2011).
6. M. J. Williamson, R. M. Tromp, P. M. Vereecken, R. Hull, F. M. Ross, *Nat. Mater.* **2**, 532 (2003).
7. H. Zheng *et al.*, *Science* **324**, 1309 (2009).
8. J. E. Evans, K. L. Jungjohann, N. D. Browning, I. Arslan, *Nano Lett.* **11**, 2809 (2011).
9. K. S. Novoselov *et al.*, *Proc. Natl. Acad. Sci. U.S.A.* **102**, 10451 (2005).
10. X. Li *et al.*, *Nat. Nanotechnol.* **3**, 538 (2008).
11. J. N. Coleman *et al.*, *Science* **331**, 568 (2011).
12. Z. Lee *et al.*, *Nano Lett.* **9**, 3365 (2009).
13. A. Kolmakov *et al.*, *Nat. Nanotechnol.* **6**, 651 (2011).
14. Y. A. Wu *et al.*, *Nanotechnology* **22**, 195603 (2011).
15. J. C. Meyer, C. O. Girit, M. F. Crommie, A. Zettl, *Appl. Phys. Lett.* **92**, 123110 (2008).
16. R. Erni *et al.*, *Phys. Rev. B* **82**, 165443 (2010).
17. R. R. Nair *et al.*, *Appl. Phys. Lett.* **97**, 153102 (2010).
18. J. M. Yuk *et al.*, *Nano Lett.* **11**, 3290 (2011).
19. K. Xu, P. Cao, J. R. Heath, *Science* **329**, 1188 (2010).
20. X. Li *et al.*, *Science* **324**, 1312 (2009).
21. W. Regan *et al.*, *Appl. Phys. Lett.* **96**, 113102 (2010).
22. X. Xie *et al.*, *Nano Lett.* **9**, 2565 (2009).
23. S. P. Koenig, N. G. Boddeti, M. L. Dunn, J. S. Bunch, *Nat. Nanotechnol.* **6**, 543 (2011).
24. J. C. Meyer *et al.*, *Nature* **446**, 60 (2007).
25. E. A. Stach, *Mater. Today* **11**, 50 (2008).
26. H. Zheng, S. A. Claridge, A. M. Minor, A. P. Alivisatos, U. Dahmen, *Nano Lett.* **9**, 2460 (2009).
27. X. Lu, M. Rycenga, S. E. Skrabalak, B. Wiley, Y. Xia, *Annu. Rev. Phys. Chem.* **60**, 167 (2009).
28. K. J. M. Bishop, C. E. Wilmer, S. Soh, B. A. Grzybowski, *Small* **5**, 1600 (2009).
29. X. Lu, M. S. Yavuz, H.-Y. Tuan, B. A. Korgel, Y. Xia, *J. Am. Chem. Soc.* **130**, 8900 (2008).
30. P. Schapotschnikow, R. Pool, T. J. H. Vlugt, *Nano Lett.* **8**, 2930 (2008).
31. Z. Z. Fang, H. Wang, *Int. Mater. Rev.* **53**, 326 (2008).

Acknowledgments: Work on preparation of a nanocrystal growth solution, portions of the design and construction of GLCs, and data analysis was supported by the Physical Chemistry of Inorganic Nanoscrystals Program, KC3105, Director, Office of Science, Office of Basic Energy Sciences, of the U.S. Department of Energy (DOE) under contract DE-AC02-05CH11231. Portions of the present study were performed at the National Center for Electron Microscopy, Lawrence Berkeley National Laboratory, which is supported by the DOE under contract no. DE-AC02-05CH11231. J.M.Y. and J.Y.L. acknowledge the financial support from Priority Research Centers Program through the National Research Foundation of Korea funded by the Ministry of Education, Science and Technology (grant no. 2010-0029714). A.Z. acknowledges support from the Director, Office of Energy Research, Office of Basic Energy Sciences, Materials Sciences and Engineering Division, of the DOE under contract DE-AC02-05CH11231, which provided for the design and construction of the GLC, and support from the Office of Naval Research under grant N00014-09-1-1066, which provided for graphene growth and spectral characterization. K.K. received further support from the NSF (grant EEC-0832819) for preliminary TEM imaging and analysis.

Supplementary Materials

www.sciencemag.org/cgi/content/full/336/6077/61/DC1
Materials and Methods
Supplementary Text
Figs. S1 to S12
References (*32*)
Movies S1 and S2

8 December 2011; accepted 27 February 2012
10.1126/science.1217654

Copper Systematics in Arc Magmas and Implications for Crust-Mantle Differentiation

Cin-Ty A. Lee,[1]* Peter Luffi,[1] Emily J. Chin,[1] Romain Bouchet,[1,2] Rajdeep Dasgupta,[1] Douglas M. Morton,[3] Veronique Le Roux,[1,4] Qing-zhu Yin,[5] Daphne Jin[1,6]

Arc magmas are important building blocks of the continental crust. Because many arc lavas are oxidized, continent formation is thought to be associated with oxidizing conditions. On the basis of copper's (Cu's) affinity for reduced sulfur phases, we tracked the redox state of arc magmas from mantle source to emplacement in the crust. Primary arc and mid-ocean ridge basalts have identical Cu contents, indicating that the redox states of primitive arc magmas are indistinguishable from that of mid-ocean ridge basalts. During magmatic differentiation, the Cu content of most arc magmas decreases markedly because of sulfide segregation. Because a similar depletion in Cu characterizes global continental crust, the formation of sulfide-bearing cumulates under reducing conditions may be a critical step in continent formation.

The composition and oxidation state of melts formed in subduction zones, collectively known as arc magmas, influence the formation and evolution of the continents, ore deposits, and possibly even the atmosphere (*1*). Arc magmas are oxidized relative to the average upper mantle; however, the means by which these lavas become oxidized is debated. The prevailing view is that arc magmas inherit their oxidized states from melting sub-arc mantle contaminated by subducted sediments and oceanic crust (*1*–*5*). Alternatively, primary arc magmas may be less oxidized than their more evolved counterparts if oxidation is caused by magmatic differentiation associated with crystallization and chemical interaction with preexisting crust (*6*–*9*).

To resolve this debate, the redox state of the mantle source regions of arc magmas must be determined. Unfortunately, primary arc magmas recording this signature are rare because by the time they have risen to the surface, they have already differentiated. One approach has been to investigate the redox state of melts trapped in phenocrysts (*4*), but melt inclusions rarely represent true primary magmas and are found only in extrusive rocks, which may not be representa-

[1]Department of Earth Science, Rice University, MS-126, 6100 Main Street, Houston, TX 77005, USA. [2]Laboratoire de Géologie de Lyon, Ecole Normale Supérieure de Lyon and Université Claude Bernard Lyon 1, CNRS UMR 5276, 46 Allée d'Italie, 69007 Lyon, France. [3]Department of Earth Sciences, University of California Riverside, 900 University Avenue, Riverside, CA 92521, USA. [4]Woods Hole Oceanographic Institution, 266 Woods Hole Road, Woods Hole, MA 02543, USA. [5]Department of Geology, University of California, Davis, CA 95616, USA. [6]William P. Clements High School, Sugar Land, TX 77479, USA.

*To whom correspondence should be addressed. E-mail: ctlee@rice.edu

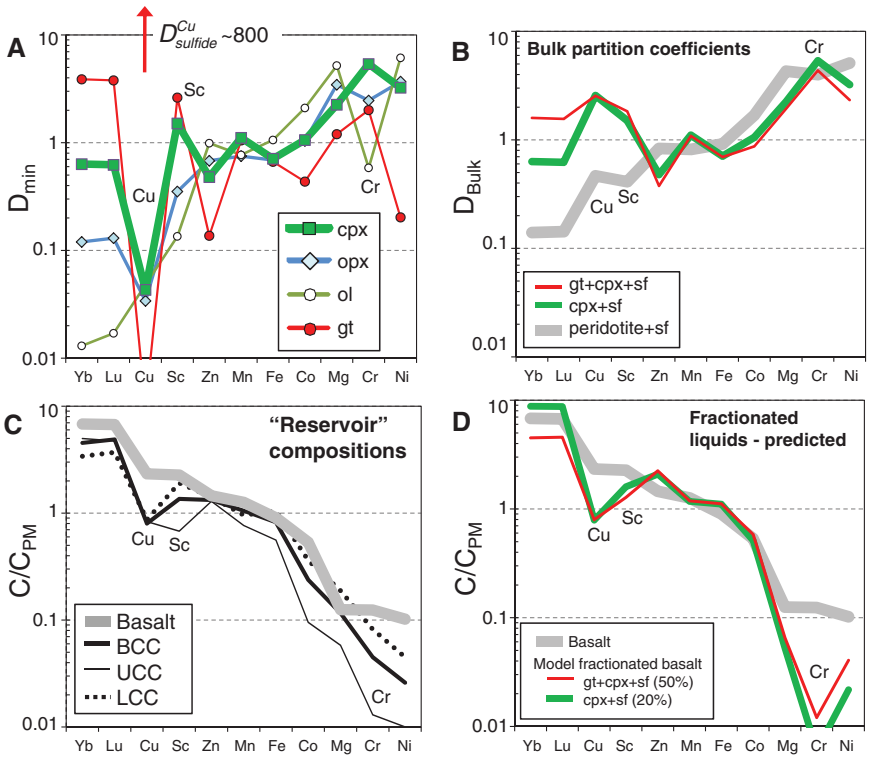

Fig. 1. (**A**) Mineral/melt partition coefficients $D_{min/melt}$ for clinopyroxene (cpx), orthopyroxene (opx), olivine (ol), and garnet (gt) plotted in order of decreasing relative abundances in MORBs. Elements with $D > 1$ and $D < 1$ are compatible and incompatible in the mineral, the latter preferentially partitioned into the melt. D values for Cu are from this study; others are taken from the literature (table S4). Cu does not fit into silicate minerals but is highly compatible in sulfide phases; value of ~800 represents partitioning of Cu between sulfide liquid and silicate liquid. (**B**) Bulk partition coefficients for peridotite (62% ol, 20% opx, and 17% cpx), clinopyroxenite, and garnet pyroxenite (30% gt and 70% cpx) containing sulfide. Sulfide mode (0.06 wt %) in peridotite is equivalent to 200 ppm S assumed for primitive mantle (*21*). Sulfide mode in pyroxenites (0.36 wt %) is defined by the solubility of sulfide in basaltic magmas undergoing fractional crystallization. (**C**) Primitive-mantle (*19*) normalized elemental abundances in basalts, based on globally averaged MORBs (for these elements, island arc basalts are similar) (*39*), and bulk, upper, and lower continental crust (BCC, UCC, and LCC) (*28*). Cu and Sc become compatible during continental crust evolution but are incompatible during mantle melting to form basalts. (**D**) Predicted residual melt compositions resulting from 50% fractional crystallization of basalt by pyroxenite and garnet pyroxenite cumulates, showing coupling of Cu and Sc depletion.

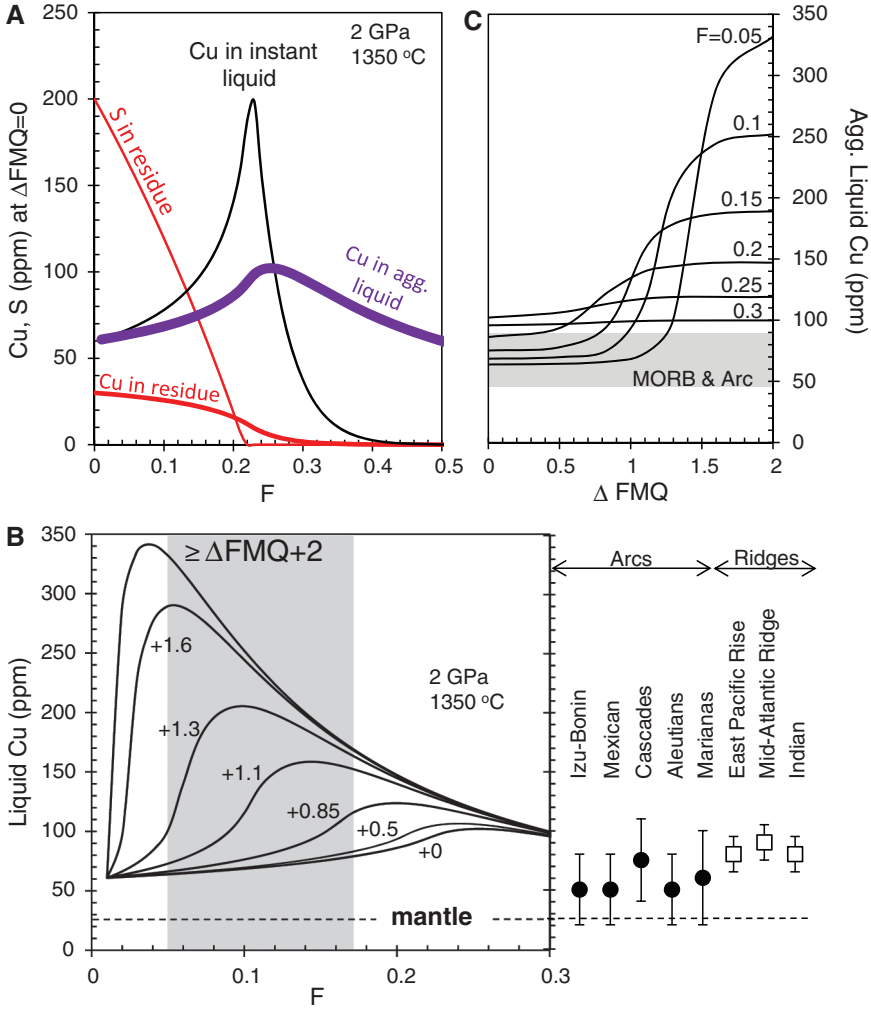

Fig. 2. Mantle melting models. (**A**) Variation of aggregated melt and residual mantle composition with degree of melting (F) at 2 GPa, 1350°C and fO_2 at FMQ+0. Initial S of 200 ppm and sulfide mode of 0.06 wt % are assumed. Melting depletes S (and sulfide) in the peridotite residue. Cu is strongly compatible in sulfide and thus moderately incompatible during early melting of peridotite, when only a small decrease in bulk Cu content in the residue occurs. After sulfide is exhausted (F = 0.2), Cu becomes highly incompatible, and its behavior is defined solely by silicate-melt partitioning. Cu content in aggregate liquid is low during initial melting and reaches a maximum at F = 0.2 when sulfide is exhausted. At $F > 0.2$, Cu decreases because of dilution. Cu content of instantaneous liquids is shown for reference. (**B**) Primary melt Cu content as a function of F and contoured against log fO_2 deviations from FMQ buffer (ΔFMQ); same P-T conditions as in (A). White squares represent MORBs from the East Pacific Rise, Indian Ridge, and Mid-Atlantic Ridge; black circles represent arc basalts from the Aleutians, Marianas, Mexico, Cascades, and Andes based on extrapolation of Cu-Mg/(Mg+Fe) trends to Mg/(Mg+Fe) = 0.72. Gray field is possible range of F in arc basalts (*40*). (**C**) Cu content of aggregate liquids versus fO_2s for different F. Gray field refers to primitive MORBs and arc Cu from (B) and Fig. 3.

tive of the entire arc crust. Another approach is to track the evolution of those metals, whose partitioning behaviors are sensitive to redox during mantle melting but largely redox-insensitive during early magmatic differentiation owing to their incompatibility in early fractionating minerals (*6*, *7*, *10*). The relative proportions of such metals then record the original redox conditions in the mantle but do not record redox evolution during differentiation.

One element that may provide insight into the entire redox history of magmas is copper (Cu). In the range of oxygen fugacities (fO_2) typical of most igneous rocks, the valence state of Cu remains +1. However, its solid/melt partitioning behavior depends on the speciation of sulfur (S) (*11*, *12*), which itself is redox-sensitive. At fO_2 values of ΔFMQ = –1 to 0 ($\log_{10}$ unit deviations from the fayalite-magnetite-quartz buffer), typical of average uppermost mantle, the dominant oxidation state is S^{2-}, which stabilizes sulfides. At high fO_2, however, S^{6+} is stable as sulfate (SO_4^{2-}) only. In silicate melts, complete conversion from sulfide to sulfate occurs within a narrow range between FMQ+1 and +2, resulting in a 10-fold increase in total S solubility (*12*). Thus, the redox state of magmas should be reflected in their S contents. However, determining pre-eruptive S contents is hampered by devolatilization of S at low pressures (*13*) as well as by post-eruptive hydrothermal alteration and weathering. Cu is strongly partitioned into sulfide minerals but is generally insensitive to such post-eruptive processes. Sulfide liquid/silicate melt partition coefficients ($D_{sf/melt}$) for Cu are between 600 and 1200 (*14*–*16*). This makes Cu a potential tracer of pre-eruptive redox state of S, provided Cu does not partition into nonsulfide phases.

To confirm that Cu partitioning into nonsulfide minerals is negligible, we measured the distribution of Cu between olivine phenocrysts and host magma and between minerals in mantle peridotites and garnet pyroxenite cumulates from arc environments (*17*). Mineral/melt partition coefficients were calculated from measured olivine/melt ($D_{ol/melt}$) and mineral/olivine partition coefficients (Fig. 1A, table S2, and fig. S1). Cu is found to be incompatible in olivine ($D_{ol/melt}$ = 0.05), orthopyroxene (0.035), clinopyroxene (0.04), amphibole (0.05), garnet (0.004), and spinel (0.2), indicating that in the presence of sulfide, the influence of these minerals on bulk partitioning of Cu is negligible (Fig. 1A). The bulk partitioning of Cu during peridotite melting $D_{per/melt}$ therefore depends on how sulfide mode varies with melt extraction. The ubiquity of sulfide-bearing peridotite samples (*18*) indicates that the mantle is generally sulfide-saturated, and detailed studies of these peridotites suggest that typical fertile mantle contains ~200 parts per million (ppm) S in the form of monosulfide solid solution (*19*–*21*). This corresponds to a sulfide mode of 0.06 weight percent (wt %) and a bulk Cu partition coefficient of ~0.5 at the onset of melting—that is, Cu is moderately incompatible, but in the absence of sulfide, Cu would be more incompatible (Fig. 1B). Thus, as melting progressively consumes sulfide, the bulk partition coefficient of Cu decreases (Fig. 2A), and when sulfide is finally exhausted, Cu becomes almost perfectly incompatible. The efficiency of S exhaustion—that is, the degree of melting needed to remove sulfide—depends on the solubility of S in the melt, which increases with decreasing pressure (*P*), increasing temperature (*T*), and increasing fO_2 (supplementary text) (*12*, *22*, *23*).

The above concepts can be quantified by modeling fractional melting of a fertile mantle

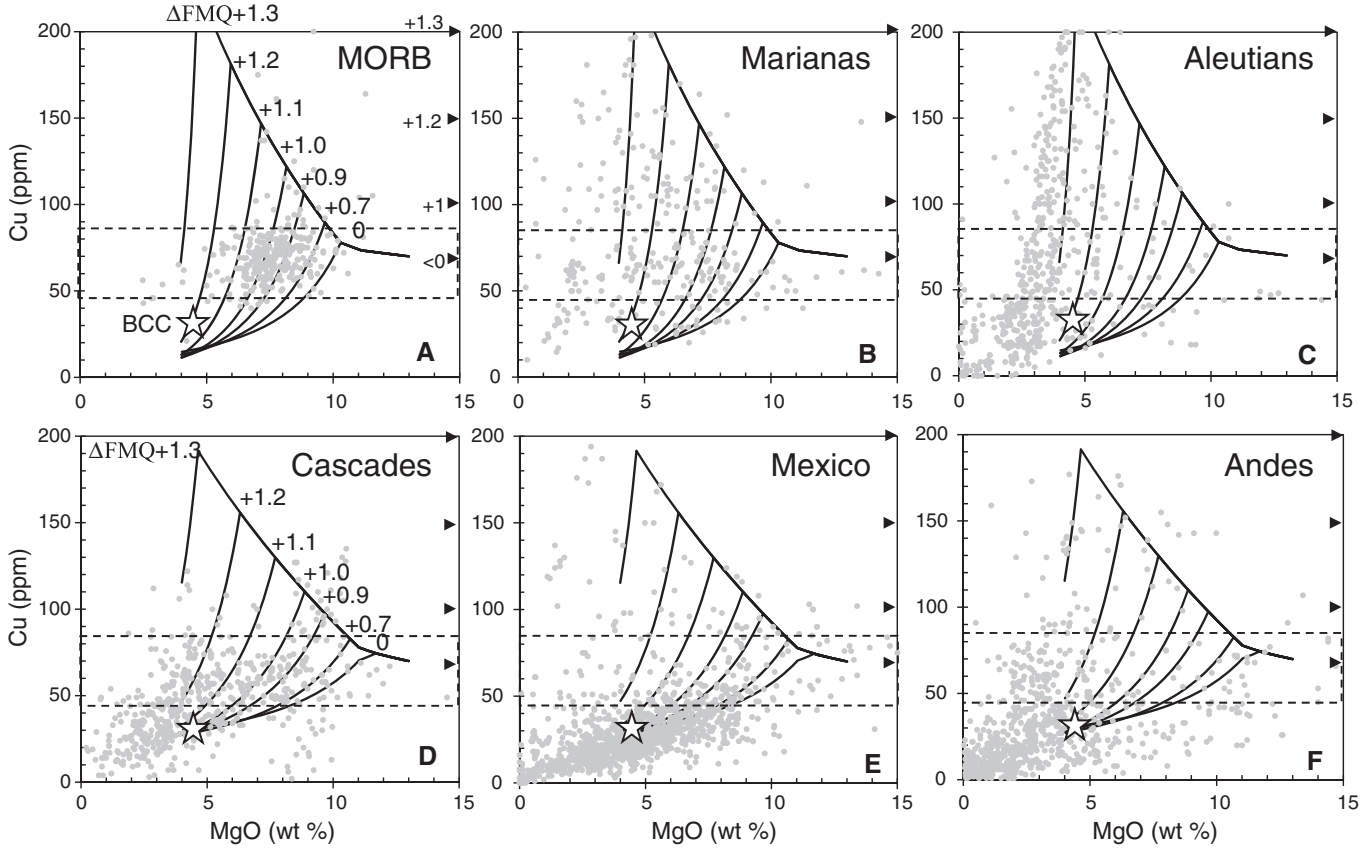

Fig. 3. Covariation of Cu and MgO in (**A**) MORB, (**B** and **C**) island arcs, and (**D** to **F**) continental arcs. Horizontal band represents average range of MORB Cu contents. Data sources are from GEOROC and RidgePetDB (supplementary text). Curves in (A) to (F) represent differentiation along fO_2 evolution paths from FMQ = 0 to the value denoted. Curves are defined by a tholeiitic fractionation series at 0.1 GPa involving olivine and plagioclase in (A) to (C) and by a calc-alkaline differentiation series at 0.8 GPa involving olivine and clinopyroxene in (D) to (F) (supplementary text). Initial starting composition is that of a primitive basalt generated at FMQ+0. Tick marks on right side of each panel show Cu in primary magma as a function of fO_2 (Fig. 2, B and C) for an average F = 0.1. Star indicates average composition of the BCC (*28*).

composition [30 ppm Cu and 200 ppm S (*19*)] to generate a series of peridotite residues and instantaneous fractional melts, which are then pooled (Fig. 2). Melts are initially enriched in Cu because $D_{per/melt} < 1$, but as melting degree F increases, sulfide mode decreases, causing $D_{per/melt}$ to decrease even further so that Cu is more efficiently transferred into the melt. A maximum Cu content in the melt is reached at $F \sim 0.2$, when all sulfide is exhausted and the system becomes sulfide-undersaturated. At higher fO_2, sulfide is exhausted at lower F, resulting in more efficient transfer of Cu into the melt (Fig. 2A, inset). For example, maximum Cu contents in melts exceed 100 ppm for FMQ+1 but are below 100 ppm for fO_2 values less than FMQ (Fig. 2A, inset). As shown in Fig. 2B, primitive (MgO > 8 wt %) mid-ocean ridge basalts (MORBs) have 60 to 70 ppm Cu and therefore cannot be explained by melting at fO_2 > FMQ (Fig. 2B). This is consistent with the generally accepted fO_2 in MORBs (*4*). More surprising is that the Cu contents of primitive arc magmas fall between 50 and 90 ppm (Figs. 2B and 3), which is indistinguishable from MORBs. This overlap suggests that the fO_2 and Cu content of sub-arc mantle must be similar to that of MORB mantle; if arc mantle had fO_2s > FMQ+1 or Cu > 40 ppm (the latter requiring enrichment by Cu-rich fluids, which in turn require high fO_2), magmatic Cu contents >200 ppm would be predicted, which is not observed. Our results are consistent with the study of Jenner *et al*. (*8*) on an individual volcanic center in the Marianas arc and require that sub-arc mantle is not highly oxidized (≤FMQ+1).

Only during magmatic differentiation does the partitioning of Cu diverge (Fig. 3). In most arcs, Cu becomes compatible during differentiation, as evidenced by monotonic decrease in Cu with decreasing MgO, an index that correlates with progressive fractional crystallization. However, in some arc magmas (mostly in island arcs) Cu initially behaves incompatibly and then increases with decreasing MgO until a maximum is reached, after which Cu becomes compatible and plummets as MgO decreases further. A quantitative understanding of these differentiation trends can be achieved by modeling the behavior of S during fractional crystallization at various fO_2 (Figs. 3 and 4). In these calculations, early crystallization sequences specific for island arcs and continental arcs were adopted (only magmas with MgO > 4 wt % were considered) in order to match major element systematics (supplementary text). Cu depletion in the magma requires sulfide segregation (probably as sulfide droplets included in fractionating silicate minerals), whereas Cu enrichment requires suppression of sulfide crystallization, which can be achieved, as mentioned above, through decompression and fO_2 increase. The divergence of Cu in arc magmas suggests different fO_2 trends during differentiation, but the fact that all arc magmatic suites eventually evolve toward highly depleted Cu contents implies that all melts ultimately reach sulfide saturation. This limits fO_2s during early magmatic differentiation to less than FMQ+1.3.

The above explanation for the depletion of Cu in evolved arc magmas predicts the formation of Cu-rich cumulates in the lower crust or lithospheric mantle. To test this prediction, we examined pyroxenite xenoliths hosted in Late Miocene basaltic volcanoes in eastern California. These pyroxenites are cumulates associated with the formation of the Cretaceous Sierra Nevada

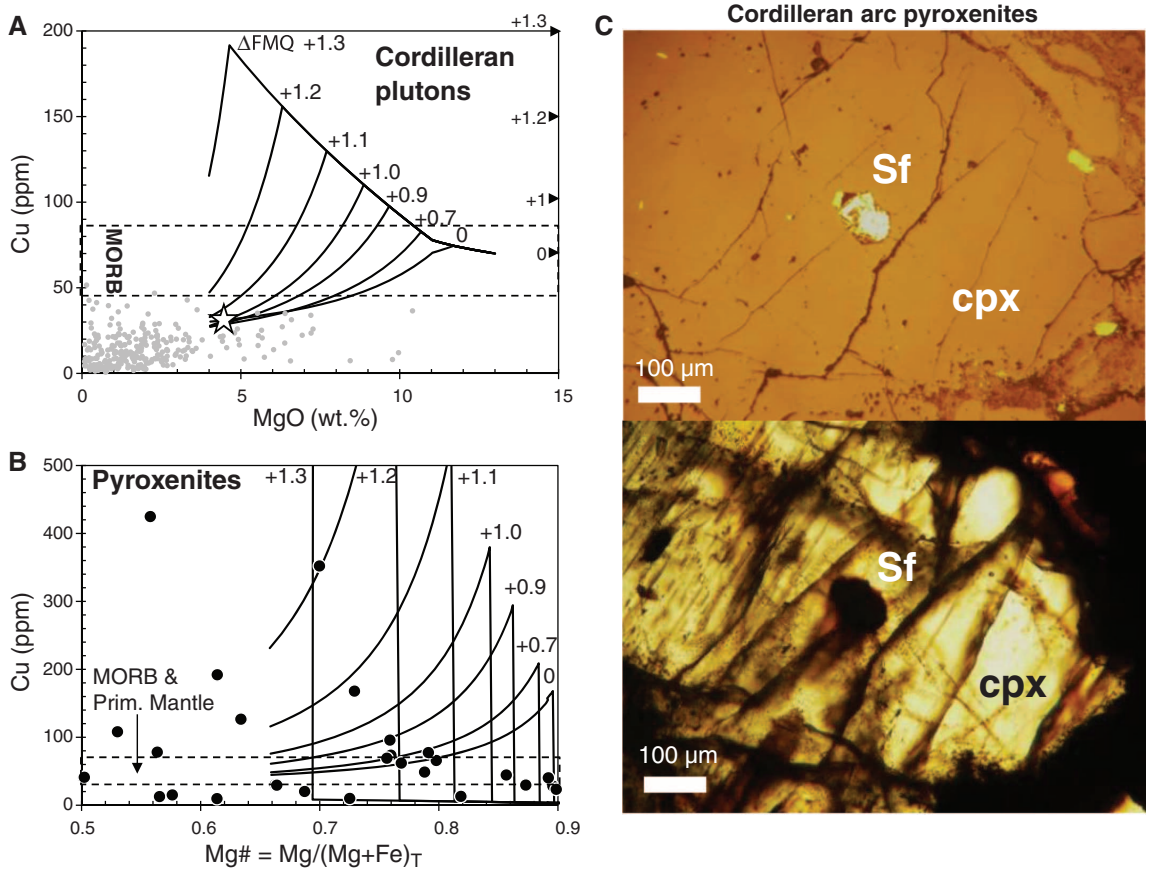

Fig. 4. Plutonic rocks and cumulates from Cretaceous Cordilleran batholiths in western North America. (**A**) Cu versus MgO in plutonic rocks from the Peninsular Ranges batholith in southern California (*27*). Curves represent evolution of mantle-derived basaltic magma during fractional crystallization of olivine-pyroxene cumulates (calc-alkaline trend) in the crust for different fO_2 values (Fig. 3, caption). (**B**) Cu versus MgO in garnet pyroxenite cumulate xenoliths from the Sierra Nevada batholith, one segment of the Cordilleran batholith. Curves represent compositions of instantaneous cumulates during fractional crystallization. These are the complements of the residual melt curves in (A). (**C**) Photomicrographs of sulfide (sf; pyrrhotite) inclusion within clinopyroxene (cpx) in the Sierran garnet pyroxenite cumulates. (Top) Reflected light. (Bottom) Unpolarized transmitted light. Star indicates BCC (*28*).

continental arc in western North America (*24*–*27*). The Cu content of the pyroxenites is highly scattered, which is expected for cumulates, particularly in continental arcs, where magma intrusion and crystallization occur through multiple events. The majority of pyroxenites is enriched in Cu compared with the primitive mantle, many containing more Cu (<400 ppm) than that of primitive basalts (70 ppm) (Fig. 4B). Both the low and high Cu abundances are consistent with our model calculations of cumulate compositions. Samples with the highest Cu contain Cu-rich sulfides (pyrrhotite and chalcopyrite) included within magmatic clinopyroxenes, which is evidence for sulfide+pyroxene co-precipitation (Fig. 4C and table S1). On the basis of the Cu content of the pyrrhotites (1 to 5 wt %) (table S3), we infer a sulfide fraction of ~1 wt % and a whole-rock S content of ~3000 ppm for the most Cu-rich pyroxenites.

The generality of the above-described behavior of Cu and S can be assessed by examining the bulk Cu systematics of the time-integrated average global continental crust. Globally averaged continental crust has ~30 ppm Cu (*28*), more than a factor of two lower than primary basaltic magmas in mid-ocean ridge and arc environments (Figs. 1C, 2, and 3A). Plotting the relative abundances of transition metals in order of compatibility during mantle melting shows that the continental crust is marked by a strong negative Cu anomaly relative to possible parental magmas, such as primitive island arc basalts or MORBs (Fig. 1C). This Cu depletion appears to be associated with depletions in scandium (Sc), chromium (Cr), and nickel (Ni). Although Ni and Cr depletion may be attributed to olivine and spinel fractionation, respectively, only clinopyroxene (and possibly amphibole) removal can simultaneously deplete Sc, Cr, and Ni (Fig. 1D). Coupled Cu and Sc depletions in global continental crust thus suggest that sulfide-pyroxenite fractionation is an important step in the evolution and formation of continents as well as arc magmas. Mass balance indicates that 70 to 80% and 20 to 30% of the original Cu and S in parental arc basalts are sequestered in such cumulates (supplementary text and fig. S3).

Our findings thus suggest that oxidizing conditions are not required to generate arc magmas or continents in general. One important implication is that the mantle source regions of arc magmas are not anomalously enriched in Cu. This may seem surprising because there is a well-known association of Cu-porphyry ore deposits with arcs (*5*, *29*). Cu-porphyries are dominantly associated with continental arcs and trace-element signatures [yttrium (Y) depletions] indicative of residual garnet (*30*), leading to the view that porphyry Cu deposits derive from mantle sources enriched in Cu via highly oxidized melting of subducted oceanic crust enriched in Cu and S during hydrothermal alteration beneath the sea floor (*5*, *31*). If, however, the mantle source is not enriched in Cu as suggested here, alternative explanations are required. Pyroxenite cumulates in the deep roots of arcs may be the only enriched source of Cu, raising the question of whether high-degree remelting of such pyroxenites can liberate, by sulfide exhaustion, the Cu necessary for forming ore deposits. Such conditions should occur when magmatic or tectonic thickening displaces cumulates to greater depths, where they are more prone to heating by the surrounding asthenospheric mantle and the passage of hot magmas. Melting at these pressures would generate peritectic garnet (*32*), resulting in magmas depleted in garnet- and clinopyroxene-compatible elements, such as Y and Sc, respectively. Although the formation of Cu-porphyry deposits still requires unusual concentration processes at shallow levels (*33*), remelting of pyroxenite cumulates in thickened arc roots may be a necessary step. Such a process may explain why porphyry Cu deposits are mainly found in thick, mature continental arcs and less in island arcs or incipient continental arcs (*34*, *35*).

What is the eventual fate of Cu-rich pyroxenite cumulates beneath arcs? Pyroxenites, especially if they have undergone metamorphic transformation into garnet pyroxenites, are denser than underlying peridotitic mantle and therefore thought to eventually founder en masse into the convecting mantle (*36*). Indeed, foundering of mafic lower crust is thought to be an important step in driving the bulk composition of continental crust toward silicic compositions (*37*). Foundering of deep arc roots may thus result in permanent removal of Cu and other sulfide-compatible metals, such as lead (Pb), from continents. This implies that formation of Cu-porphyries may be possible only in a narrow window within the history of a continental arc (fig. S4) (*38*). Last, because Pb is the daughter product of uranium, which itself is not partitioned into sulfide-bearing pyroxenites, foundering of these pyroxenites through Earth's history could have generated an unradiogenic Pb isotope reservoir deep in the mantle, leaving behind a continental crust and upper mantle characterized by radiogenic Pb isotopes.

References and Notes

1. R. J. Arculus, *Annu. Rev. Earth Planet. Sci.* **13**, 75 (1985).
2. J. B. Gill, *Orogenic Andesites and Plate Tectonics* (Springer, Berlin, 1981).
3. I. S. E. Carmichael, *Contrib. Mineral. Petrol.* **106**, 129 (1991).
4. K. A. Kelley, E. Cottrell, *Science* **325**, 605 (2009).
5. J. E. Mungall, *Geology* **30**, 915 (2002).
6. C.-T. A. Lee *et al.*, *Nature* **468**, 681 (2010).
7. C.-T. A. Lee, W. P. Leeman, D. Canil, Z.-X. A. Li, *J. Petrol.* **46**, 2313 (2005).
8. F. Jenner, H. S. C. O'Neill, R. J. Arculus, J. Mavrogenes, *J. Petrol.* **51**, 2445 (2010).
9. N. Dauphas *et al.*, *Earth Planet. Sci. Lett.* **288**, 255 (2009).
10. D. Canil, *Nature* **389**, 842 (1997).
11. P. J. Jugo, *Geology* **37**, 415 (2009).
12. P. J. Jugo, M. Wilke, R. E. Botcharnikov, *Geochim. Cosmochim. Acta* **74**, 5926 (2010).
13. P. J. Wallace, *J. Volcanol. Geotherm. Res.* **140**, 217 (2005).
14. E. M. Ripley, J. G. Brophy, C. Li, *Geochim. Cosmochim. Acta* **66**, 2791 (2002).
15. S. J. Lynton, P. A. Candela, P. M. Piccoli, *Econ. Geol.* **88**, 901 (1993).
16. G. A. Gaetani, T. L. Grove, *Geochim. Cosmochim. Acta* **61**, 1829 (1997).
17. Materials and methods are available as supplementary materials on *Science* Online
18. M. R. Handler, V. C. Bennett, G. Dreibus, *Geology* **27**, 75 (1999).
19. W. F. McDonough, S.-S. Sun, *Chem. Geol.* **120**, 223 (1995).
20. J.-P. Lorand, *Earth Planet. Sci. Lett.* **93**, 50 (1989).
21. J. P. Lorand, *Geochim. Cosmochim. Acta* **54**, 1487 (1990).
22. J. A. Mavrogenes, H. S. C. O'Neill, *Geochim. Cosmochim. Acta* **63**, 1173 (1999).
23. H. S. C. O'Neill, J. A. Mavrogenes, *J. Petrol.* **43**, 1049 (2002).
24. M. N. Ducea, *J. Geophys. Res.* **107**, (B11), 2304 (2002).
25. M. N. Ducea, J. B. Saleeby, *Contrib. Mineral. Petrol.* **133**, 169 (1998).
26. C.-T. A. Lee, X. Cheng, U. Horodyskyj, *Contrib. Mineral. Petrol.* **151**, 222 (2006).
27. C.-T. A. Lee, D. M. Morton, R. W. Kistler, A. K. Baird, *Earth Planet. Sci. Lett.* **263**, 370 (2007).
28. R. L. Rudnick, S. Gao, *Treatise Geochem.* **3**, 1 (2003).
29. J. Richards, *Geology* **37**, 247 (2009).
30. J. P. Richards, R. Kerrich, *Econ. Geol.* **102**, 537 (2007).
31. R. Oyarzun, A. Marquez, J. Lillo, I. Lopez, S. Rivera, *Miner. Depos.* **36**, 794 (2001).
32. R. Alonso-Perez, O. Müntener, P. Ulmer, *Contrib. Mineral. Petrol.* **157**, 541 (2009).
33. J. W. Hedenquist, J. B. Lowenstern, *Nature* **370**, 519 (1994).
34. D. R. Cooke, P. Hollings, J. L. Walshe, *Econ. Geol.* **100**, 801 (2005).
35. R. H. Sillitoe, *Econ. Geol.* **105**, 3 (2010).
36. M. Jull, P. Kelemen, *J. Geophys. Res.* **106** (B4), 6423 (2001).
37. R. L. Rudnick, *Nature* **378**, 571 (1995).
38. M. Haschke, J. Ahmadian, M. Murata, I. McDonald, *Econ. Geol.* **105**, 855 (2010).
39. R. Arevalo Jr., W. F. McDonough, *Chem. Geol.* **271**, 70 (2010).
40. K. A. Kelley *et al.*, *J. Geophys. Res.* **111** (B9), B09208 (2006).

Acknowledgments: This work was funded by an NSF grant to C.-T.A.L. Discussions with F. Albarede, J. Blichert-Toft, S. Huang, D. Anderson, R, Rudnick, W. McDonough, and R. Arevalo are appreciated. D.J.'s participation in this project was made possible by F. Steinkamp's Scientific Research and Design course at William P. Clements High School in Sugar Land, TX. All data are available in the supplementary materials. C.-T.A.L. planned the research and wrote the manuscript. E.J.C. collected the whole-rock data for Sierran garnet pyroxenites. R.B. collected the olivine phenocryst-groundmass trace-element data. C.-T.A.L. and P.L. collected the mineral/mineral trace-element partition coefficients in peridotites, pyroxenites, and sulfides. D.J. developed the ideas behind Fig. 1C. All authors participated in interpretation of the data and modeling.

Supplementary Materials

www.sciencemag.org/cgi/content/full/336/6077/64/DC1
Materials and Methods
Supplementary Text
Figs. S1 to S4
Tables S1 to S4
References (*41*–*67*)

30 November 2011; accepted 28 February 2012
10.1126/science.1217313

www.sciencemag.org/cgi/content/full/336/6077/64/DC1

Supplementary Material for

Copper Systematics in Arc Magmas and Implications for Crust-Mantle Differentiation

Cin-Ty A. Lee,* Peter Luffi, Emily J. Chin, Romain Bouchet, Rajdeep Dasgupta, Douglas M. Morton, Veronique Le Roux, Qing-zhu Yin, Daphne Jin

*To whom correspondence should be addressed. E-mail: ctlee@rice.edu

Published 6 April 2012, *Science* **336**, 64 (2012)
DOI: 10.1126/science.1217313

This PDF file includes:

Other Supplementary Material for this manuscript includes the following:
(available at www.sciencemag.org/cgi/content/full/336/6077/64/DC1)

Tables S1 to S4 as an Excel file
Program-Chalcophile as an Excel file

Materials and Methods

Samples

Cu and major-element data for plutonic rocks from the Cretaceous Peninsular Ranges batholith in the North American Cordillera are taken from Lee et al. (*41*). We also present new and published (*41, 42*) Cu data for garnet pyroxenite xenoliths from late Miocene basaltic diatremes that erupted through the Sierra Nevada batholith, another segment of Cretaceous North American Cordilleran batholiths (Table S1). The petrogenesis of these pyroxenites have been discussed elsewhere (*41-46*); they are generally agreed to represent deep-seated restites and cumulates associated with plutonism in the Sierra Nevada batholith. These pyroxenites are dominated by clinopyroxene and garnet, but some samples contain primary amphiboles or orthopyroxene.

We used in situ laser ablation ICP-MS to determine the Cu content of minerals in the above pyroxenites as well as in a wide spectrum of peridotites (Table S2). These included spinel and garnet-peridotite xenoliths from various localities in western USA (Simcoe in WA; Grand Canyon and San Carlos in AZ; Cima, Dish Hill, Oak Creek and Big Creek in CA; Lunar Crater, NV; Persani Mountains in Romania; Letlhakane kimberlite in Botswana and Venetia kimberlite in South Africa). We also analyzed minerals in harzburgites from the Josephine ophiolite in California. Sulfide mineral compositions in the pyroxenites were also analyzed (Table S3). Phenocryst and magma groundmass pairs were used to determine olivine/melt partition coefficients. We used olivine-bearing basalts from the San Joaquin and Big Pine volcanic fields in California and the Mount Trumbull volcanic field on the north rim of the Grand Canyon in Arizona (USA). Groundmass compositions were determined by averaging multiple large (110 μm) spot analyses with laser ablation ICP-MS.

Cu and major-element data for mid-ocean ridge basalts and arc magmas (from basalts to andesites) were taken from the RidgePetDB (http://www.petdb.org/) and GEOROC databases http://www.**georoc**.mpch-mainz.gwdg.de), respectively. These data are provided with this manuscript for reference. This is the same dataset used in Lee et al. (*47*).

Methods

Whole-rock data for Sierran pyroxenites were determined by XRF at Washington State University, Pullman and solution ICP-MS at Rice University, the latter following methods detailed in Li and Lee (*48*) (Table S1). Cu contents of individual minerals were determined by laser ablation ICP-MS at Rice University using a 213 nm New-Wave laser ablation introduction system coupled to a ThermoFinnigan Element 2 magnetic sector ICP-MS (Table S2). Analytical details have been published elsewhere (*49*). Cu was determined by measuring ^{63}Cu in medium mass resolution ($m/\Delta m$ =3000) in order to resolve against molecular interferences on mass 63. In medium mass resolution, all major element metals were also monitored (^{23}Na, ^{25}Mg, ^{28}Si, ^{27}Al, ^{39}K, ^{43}Ca, ^{49}Ti, ^{55}Mn, ^{57}Fe) in order to obtain an internal standard for normalization following Lee et al. (*49*). Ratios of signal intensities between two elements were converted to concentrations by normalizing against a calibration curve using three external glass standards (United States

Geological Survey BHVO-2g, BIR-1g, and BCR-2g) and the standard values from Gao et al. (*50*).

We also measured the metal contents in sulfide minerals in the pyroxenites by laser ablation ICP-MS (Table S3). This was done by measuring ^{55}Mn, ^{59}Co, ^{63}Cu, ^{60}Ni, ^{66}Zn, ^{57}Fe, ^{33}S, ^{95}Mo, ^{105}Pd, ^{109}Ag, and ^{195}Pt isotopes. Signals were normalized to Fe and the metal or S/Fe ratios were converted to concentration ratios using external standards (this approach is suitable if the material is a pure sulfide; if the material analyzed also contains oxides, the absolute abundance will be under-estimated because O is not accounted for). For S, we used a stoichiometric sample of pyrite. For all other elements we used pyrite (for Fe only) and two iron meteorites as standards (Hoba and Filomena; standard values given in Campbell et al. (*51*)). These concentration ratios normalized to Fe were then converted to absolute concentrations by summing all metals and S to 100%. Estimated uncertainties are 10%. Many of these sulfides occur as polymineralic aggregates consisting of pyrrhotite, pyrite and chalcopyrite and secondary Fe-oxides (the latter likely breakdown products of the sulfides during entrainment of the pyroxenite xenoliths in the erupting magmas). Because many of these aggregates are small (comparable to our laser spot size of 40-100 µm diameter), these heterogeneities could not be resolved. As a consequence of this heterogeneity and of our approach of normalizing metal and S contents to 100 % (and ignoring O), the atomic proportions of metals to S did not always match a pure sulfide. These issues should be taken into consideration when examining the Fe and S data in Table S3. For Cu and other trace metals, however, the 10 % uncertainty is sufficient for the purposes of this study.

SOM Text

Partition coefficients

Olivine/melt partition coefficients for Cu were determined using phenocryst and groundmass compositions in basalts from the Basin and Range province in western USA (Tables S2 and S4). Only phenocryst-groundmass pairs that showed equilibrium Co/Mn and Zn/Mn exchange coefficients were used (values were taken from (*52, 53*)). Based on the high MgO content of these basalts (>8 wt. %), crystallization temperatures are >1150 C. Cu partition coefficients for orthopyroxene, clinopyroxene and spinel were then determined by multiplying olivine/melt partition coefficients with orthopyroxene/olivine, clinopyroxene/olivine, garnet/olivine and spinel/olivine partition coefficients measured in peridotites (Tables S2 and S4). This approach is similar to how Le Roux et al. (*53*) determined Zn partition coefficients for these minerals. Garnet/melt partition coefficients were also determined indirectly from garnet-pyroxenite xenoliths from the Sierra Nevada (*42*) by multiplying clinopyroxene/melt by measured garnet/clinopyroxene partition coefficients. In a similar fashion, amphibole-bearing pyroxenite xenoliths were used to obtain amphibole/melt partition coefficients. Given that the peridotite samples have very different equilibration temperatures and pressures, the strong correlation of Cu between mineral phases (Fig. S1a) indicates that these mineral/mineral partition coefficients are, to within error, not strongly sensitive to temperature and therefore, we can use these mineral/mineral coefficients to infer mineral/melt partitioning using the olivine/melt partitioning measurements described above.

We estimate olivine/silicate melt partition coefficients of 0.048 and because the mineral/mineral partition coefficients are ~1, this implies that Cu is incompatible in all the silicate minerals and oxides (spinels) of interest (Tables S2 and S4). We note that Cu partition coefficients in the Geochemical Earth Reference Model database (GERM; http://earthref.org/GERM/) range from 0.03 to 3 for olivine/, orthopyroxene/, and clinopyroxene/melt partition coefficients, but much of this variation is because old phenocryst-magma studies required mechanical separation of phenocrysts from groundmass, making it difficult to avoid inclusions and other heterogeneities within the phenocryst. Our in situ approach here, combined with our approach in assessing equilibrium between phenocryst and groundmass, is more robust at obtaining true equilibrium partition coefficients.

Additional partition coefficients used in this study were obtained as follows. Olivine/melt and orthopyroxene/melt partition coefficients for Yb and Lu were taken from Lee et al. (*54*), which were determined to be internally consistent with clinopyroxene/melt and garnet/melt Yb partition coefficients of Hauri et al. (*55*) at 2.5 GPa and 1430 °C. Sc mineral/melt partition coefficients for olivine, orthopyroxene, clinopyroxene, and spinel were taken from Mallmann and O'Neill (*56*) at 1300 °C. Sc partitioning for garnet was taken from Hauri et al. (*55*). Partition coefficients for Zn, Mn, Fe, and Co were taken from Le Roux et al. (*52*). Mg partitioning for olivine, orthopyroxene, and clinopyroxene were taken from Takahashi (*57*) at 1 GPa and 1325 °C. Mg partitioning for garnet was taken from Walter (*58*) at 4 GPa and 1540 °C; this is at a higher temperature than used for the other partition coefficients, but because Mg is so compatible in olivine and pyroxenes compared to garnet, the effect of garnet on bulk Mg partitioning in peridotites is small. Cr partitioning in olivine, orthopyroxene, clinopyroxene, and spinel were taken from Mallmann and O'Neill (*56*) and in garnet from Hauri et al. (*55*). Ni partition coefficients for olivine, orthopyroxene, and clinopyroxene were taken from Le Roux et al. (*52*). Garnet Ni partition coefficients were calculated by multiplying olivine/melt partition coefficients by garnet/olivine partition coefficients extrapolated to 1350 °C using the parameterizations of Griffin et al. (*59*).

We attempted above to compile an internally consistent set of partition coefficients for basaltic systems at upper mantle temperatures and pressures (>1 GPa and 1300-1450 °C). These partition coefficients should not be applied to crystal fractionation at lower temperatures or to more evolved magmas, such as andesites.

Melting calculations

The Cu and S contents of primary mantle-derived magmas are determined from melting models of peridotite at upper mantle conditions. The assumed mineralogy is 62% ol, 20% opx, 17% cpx, and 1% spinel but because we are interested in Cu, which is primarily controlled by sulfide, variations in silicate and spinel modes are not important. We assume near-fractional melting, which we approximate by removing equilibrium (e.g., batch) melts at small increments and updating the composition of the peridotite residue accordingly. The starting composition is a mantle peridotite with 200 ppm S, all of which is stored in the sulfide phase. We assume that the sulfide phase in mantle rocks is sulfide liquid with a monosulfide solid solution composition, e.g., (Fe,Ni)S, corresponding to 360,000 ppm S in the sulfide phase. The mode of sulfide in the peridotite at any given stage *i* in the melting process is

$$X_{Sf}^{i} = \frac{C_{S,per}^{i}}{C_{S,sf}^{i}} \quad (1)$$

For example, a primitive mantle of 200 ppm S contains 0.06 wt % of sulfide. The S content of the residue (solid minerals and sulfide liquid) and the silicate melt are controlled by the solubility of S in the silicate melt, which is defined at a given T, P, oxygen fugacity (fO_2) and major element composition of the melt. If these variables are constant, then S in the melt is buffered at a constant value as long as the sulfide is present in the residue. At low fO_2 (<FMQ-1), all S in the melt is in the S^{2-} redox state. The S content $C_{S,melt}$ under these conditions is given by (*60*)

$$\ln C_{S^{2-},melt} = \frac{A}{T} + B + \frac{CP}{T} + \ln a_{FeS}^{Sf} \quad (2)$$

Where $C_{S,melt}$ is in ppm, T is in Kelvin, P is in bars, and a_{FeS}^{Sf} is the activity of FeS in the sulfide, which we assume to be ~1 (A, B, and C are -6684, 11.52 and -0.047). Eq. 2 indicates that S solubility increases with increasing T and decreasing P. There is an additional effect of the FeO_T content of the melt (*61*), but we assume that the FeO_T content of our mantle melts are between 8-10 wt. %, similar to that used to calibrate the above equation, and thus we do not incorporate this effect. The effect of fO_2 on S_T solubility is accounted for by tracking the speciation of S in the melt as a function of fO_2, e.g., the atomic proportion S^{6+}/S_T (where total S is $S_T = S^{6+} + S^{2+}$). We adopt the most recent formulation of Jugo et al. (*62*)

$$\frac{S^{6+}}{S_T} = \frac{1}{1+10^{2.1-2\Delta FMQ}} \quad (3)$$

where ΔFMQ is the deviation of fO_2 from the fayalite-magnetite-quartz buffer in $\log_{10}$ units. This equation shows that at high fO_2, S^{6+}/S_T approaches 1. At low fO_2 (e.g., negative values of FMQ), S^{6+}/S_T approaches 0, corresponding to a S^{2-} dominated system. Eq. 3 can be re-arranged to yield to the total S content S_T in the melt as a function of fO_2 (*62*)

$$C_{S_T,melt} = C_{S^{2-},melt}\left(1+10^{2\Delta FMQ-2.1}\right) \quad (4)$$

where $C_{S^{2-},melt}$ is the S concentration of the melt for the case in which S^{6+}/S_T =0 (or fO_2 is low). Eqs. 2 and 4 can then be combined to estimate the total S content S_T of the melt at a given T, P and fO_2:

$$C_{S_T,melt} = \left(1+10^{2\Delta FMQ-2.1}\right)\exp\left(\frac{-6684}{T} + 11.52 - \frac{0.047P}{T} + \ln a_{FeS}^{Sf}\right) \quad (5)$$

The fractional melting process in the mantle is ultimately the by-product of adiabatic decompression melting. However, for simplicity, we assume an average effective pressure and temperature of melting representative of partial melting conditions in the asthenospheric mantle wedge. For melting beneath mid-ocean ridges and incipient arcs, we assume T = 1350 °C, P = 1.5 GPa. For melting beneath mature arcs in subduction zones, we assume 1350 °C and 2 GPa. The concentration of S in the peridotite residue at any given stage of the melting process is

$$C_{S,per}^{i+1} = \frac{M_i C_{S,per}^{i} - C_{S,melt}^{i} \Delta M}{M_{i+1}} \quad (6)$$

where *i* corresponds to a given step in the melting process, *M* is the mass of the peridotite residue at step *i* or *i+1*. ΔM is the mass of melt extracted between stage *i* and *i+1* (i.e., M_{i+1}-M_i). Progressive melting leads to the depletion of S (and sulfide) in the peridotite residue. The rate of S depletion in the residue depends on the solubility of S in the melt. For our purposes, fO_2 is the most important variable. At high fO_2, S solubility in the melt is much higher than at low fO_2, resulting in more rapid depletion of S in the peridotite residue. An obvious property is that the behavior of S does not depend on the silicate and oxide mineralogy because S is controlled exclusively by sulfides (or sulfates at high fO_2).

The above models of S and sulfide evolution in the melt and peridotite residue are used to track the melting behavior of chalcophile trace-elements, such as Cu and Pb. The distribution of Cu between peridotite and melt at any instant is controlled by equilibrium partitioning, which itself varies because the mineralogy of the peridotite residue, particularly the sulfide mode, changes with progressive melt extraction. Defining the mineral/melt equilibrium partition coefficient as $D_{j/melt} = C_j / C_{melt}$, the bulk peridotite/melt partition coefficient at step *i* of the melting process is

$$D_{per/melt}^{i} = \sum_j X_j^i D_{j/melt} \quad (7)$$

where X_j^i is the mode of a given phase within the peridotite at stage *i*. For chalcophile elements, $D_{sf/melt}$ is much larger than that of any silicate phases and therefore $D_{per/melt}^{i}$ depends primarily on X_{sf}^{i}. In other words, variations in the relative abundances of silicate phases are again negligible for modeling chalcophile elements. Because X_{sf} decreases with progressive melt extraction, the bulk partition coefficient of a chalcophile element, i.e., $D_{per/melt}$, also decreases and eventually becomes zero (perfectly incompatible) when sulfide is exhausted. Depending on the magnitude of $D_{sf/melt}$, the effect of progressive melting on the bulk partition coefficient of a chalcophile element can be profound. For example, Cu has a $D_{sf/melt}$ ~800 (*63*), which means that in the beginning of melting, Cu behaves in bulk as a moderately incompatible element, but with progressive melting, it becomes highly incompatible and is efficiently removed from the peridotite. For elements with $D_{sf/melt}>10^4$, such as the case for platinum group elements, these elements behave compatibly during the early stages of melting, becoming incompatible only when very high degrees (>30 %) of melting are achieved (Fig. S2). In detail, the concentration of a given trace-element in each melt increment (i.e., the instantaneous melt) is given by

$$C_{melt}^{i+1} = \frac{C_{per}^{i}}{D_{per/melt}^{i} + \left(1 - D_{per/melt}^{i}\right)\Delta M / M_i} \quad (8)$$

where symbols are defined as in previous equations. The concentration of the trace-element in question in the residue at step *i+1* is given by

$$C_{per}^{i+1} = \frac{\left(C_{per}^{i} M_i - C_{melt}^{i+1} \Delta M\right)}{M_{i+1}} \quad (9)$$

In practice, individual melt increments have been shown to eventually aggregate before they erupt. For these reasons, we pool all melt increments to yield an aggregate melt composition whose chalcophile trace-element and S contents represent a weighted average of all melt increments. For a typical incompatible element, whose bulk compatibility does not change substantially with melting degree, its concentration in the aggregate melt decreases with increasing melting degree due to the effect of dilution and, for our purposes, can be modeled by a single batch melting equation. However, for chalchophile elements, the strong effect of varying sulfide mode on the bulk partition coefficient leads to non-intuitive behavior. The concentration of Cu, for example, in aggregate melts first increases with melting degree because Cu becomes more incompatible, but as the Cu content in the peridotite residue decreases, subsequent melt increments inherit this Cu-depleted signature, which leads to dilution of the Cu in the aggregate melt. Thus, unlike lithophile incompatible trace-elements, whose concentrations in the melt decrease monotonically, that of a chalcophile element exhibits a distinct maximum at a characteristic melting degree.

The melting routine is provided as an Excel spreadsheet.

Fractional crystallization calculations

To model fractional crystallization in arc settings, we take the F=10% aggregate melt from the partial melting models above as the initial melt composition. We assume that the melts generated at mantle depths (1.5 GPa for mid-ocean ridges and island arcs; 2 GPa for continental arcs, ~60 km) rise adiabatically into the crust, upon which the melts stall, cool and crystallize isobarically (0.1 GPa for mid-ocean ridges and island arcs; 1 GPa for continental arcs). We assume that all precipitating phases, such as silicate crystals as well as sulfide liquid droplets, gravitationally segregate owing to their high densities compared to the silicate melt. Such segregation leads to fractional crystallization, which we model as an incremental process. We assume that crystallization follows the crystal line of descent seen in natural magmatic differentiation series. To model a calc-alkaline differentiation trend, typifying continental arcs, we assumed wehrlite (60 % cpx, 40 % ol) fractionation for the first 10 % of fractionation, followed by clinopyroxenite fractionation until a MgO content of 4 wt. % was reached in the residual magma. We also model a tholeiitic differentiation trend, which typifies mid-ocean ridges and some island arcs: olivine for the first 5 % of fractionation, plagioclase (50 %) and olivine (50%) for the next 5%, and olivine (20 %), plagioclase (50%) and clinopyroxene (30%) until 4 wt. % MgO is reached.

Because crystal fractionation and T decrease go hand-in-hand to first order, the effect of decreasing temperatures on solubility of S in the magma must be accounted for. We track temperature by tracking the evolution of MgO in the liquid and using MgO-liquid based thermometers (*64*). Because much of the crystal line of descent involves clinopyroxene fractionation, FeO contents in the melt increase slightly with progressive crystal fractionation. Increasing FeO increases S solubility (*60, 61*), so the FeO content of the melt and its effect on S solubility was also accounted for (although over the range of FeO contents modeled, this effect is small). An important feature of decompression is that regardless of the fO_2, the low P at which crystallization takes place compared to the original melting P renders all magmas initially under-saturated in S. Thus, S and any chalcophile elements in the magma will initially increase during fractional crystallization

until the S content saturates. Once saturation is reached, a sulfide phase (or sulfate phase if fO_2 is high enough) forms and is assumed to segregate gravitationally, that is, fractionate. After this point, the S content in the melt is dictated by S solubility at the given P, T and fO_2, while the chalcophile element concentration in the magma is progressively depleted. S solubility in the magma follows the same equations as described above for melting. The relevant equations for modeling chalcophile element distribution in the melt and cumulates are described as follows. The proportion of sulfide phase X_{Sf}^{i+1} in the segregating assemblage at a given stage in the incremental fractionation process is given by

$$X_{Sf}^{i+1} = \frac{C_{S,melt}^{i} \Delta M / M_i}{C_{S,Sf}^{i}} \tag{10}$$

where ΔM is the mass increment of fractionating products in a given step, $C_{S,melt}^{i}$ is the concentration of S in the magma, $C_{S,Sf}^{i}$ is the concentration of S in the sulfide (assumed to be of pyrrhotite composition, which we approximate as FeS), and M_i is the mass of the residual magma at step *i*. All other fractionating phases are silicates (olivine and pyroxenes). The concentration of S in an instantaneous cumulate is given by

$$C_{S,cum}^{i} = X_{Sf}^{i} C_{S,Sf}^{i} \tag{11}$$

The concentration of a chalcophile trace-element in the cumulate at step *i+1* is given by

$$C_{cum}^{i+1} = \frac{D_{cum/melt}^{i} C_{melt}^{i+1}}{M_{i+1}/M_i - D_{cum/melt}^{i} \Delta M / M_i} \tag{12}$$

where $D_{cum/melt}^{i}$ represents the bulk partition coefficient between cumulates and melt defined using Eq. 7. All other symbols are defined as above.

The above equations are used to track the evolution of the residual magma and the instantaneous cumulates at each increment *i* of sulfide liquid and silicate crystal fractionation (Fig. S3). We also model how Mg# (atomic $Mg/(Mg+Fe_T)$) of the residual magma and cumulates change with fractionation degree. This is done by incrementally removing the silicate mineral phases along with sulfide. At each increment, we assume Fe-Mg equilibrium between silicate phases and silicate melt (an equilibrium Fe/Mg exchange coefficient $K_D^{Fe/Mg} = (Fe/Mg)^{\min}/(Fe/Mg)^{melt}$ of 0.3 for olivine and 0.29 for clinopyroxene) and stoichiometry (i.e., $(Mg,Fe)_2SiO_4$ and $Ca(Mg,Fe)Si_2O_6$) to track the evolution of MgO and FeO in the silicate melt. Fe in the silicate melt is assumed to be Fe^{2+} (for the purposes of this study, the effect of fO_2 on Fe/Mg K_D is not important).

The fractionation routine is provided as an Excel spreadsheet.

Estimating proportions of Cu, S and Pb missing from arc magmas

The above models for fractional crystallization can also be used to estimate the mass fraction *f* of Cu, S and Pb missing from the continental crust and stored in pyroxenite cumulates. This can be estimated using the following equation

$$f = \frac{C_{cum} M_{cum}}{C_{melt}^{o}} \tag{13}$$

where C_{cum} is the concentration of the element of interest in the *aggregate* cumulate, C_{melt}^{o} is the initial concentration in the melt (e.g., the primary magma), and M_{cum} is the

total mass of the cumulates. We have performed one calculation at FMQ. The mass proportions of missing Cu, S, and Pb are plotted in Fig. S3 as a function of Cu content in the residual magma. Such a figure allows one to use the Cu content of average continental crust or arc crust to infer the amount of missing Cu, S or Pb. For a primary magma with 70 ppm Cu and a Cu content of 30 ppm for average continental crust, we find that ~85% of Cu, 50% of S, and 5% of Pb are missing from the original parental basaltic magma. The differences in these numbers are ultimately related to the overall compatibility of these elements during magmatic differentiation, that is, $D_{Cu}>D_S>D_{Pb}$. We have used a $D_{sulfide}$ for Pb of 14 from Hart and Gaetani (*65*); had we used a higher partition coefficient, such as an upper bound of 40 in Hart and Gaetani, f_{Pb} would have been higher (15%). In either case, our results for Pb are consistent with observations. Most of the Pb in the bulk silicate Earth is ultimately stored in the continental crust, as is well-known (*66*), but enough Pb is stored in sulfide-bearing cumulates to make this an important reservoir in the mantle. We also note that our estimated amount of missing Cu does not include all the Cu that might be stored in Cu-porphyry ore deposits. However, Wilkinson and Kessler (*67*) showed that these ore deposits make up only 0.25 % of the total crustal budget of continental crust, underscoring how rare such deposits are. As stated in the main text, the re-melting of Cu-rich pyroxenites occurs when the arc crust is thick. Foundering of this arc crust would remove the pyroxenites, hence re-melting of pyroxenites occurs in a narrow window of time (Fig. S4).

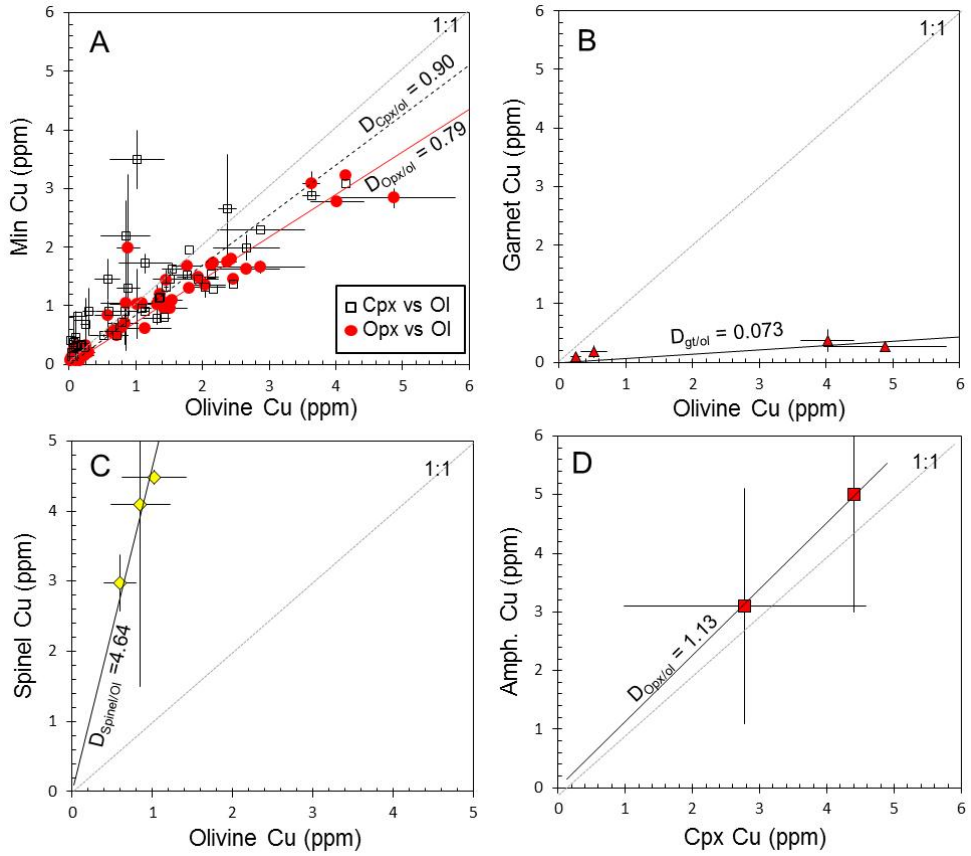

Fig. S1.

Cu concentration data in co-existing mineral phases in peridotites and pyroxenites. A) Cu in clinopyroxene and orthopyroxene versus Cu in coexisting olivine. Labeled lines represent linear regressions forced through zero. The slope gives the apparent mineral/mineral partition coefficient. Dotted line represents a 1:1 line for reference, where Cu would be equally partitioned into both phases. B) Cu in garnet versus Cu in olivine. C) Cu in spinel versus Cu in olivine in spinel peridotites. D) Cu in primary amphiboles versus Cu in clinopyroxene in garnet-clinopyroxenite xenoliths from the Sierra Nevada. Error bars represent 2 standard deviations of multiple analyses (Table S1). When no error bar is shown, only one analysis was performed.

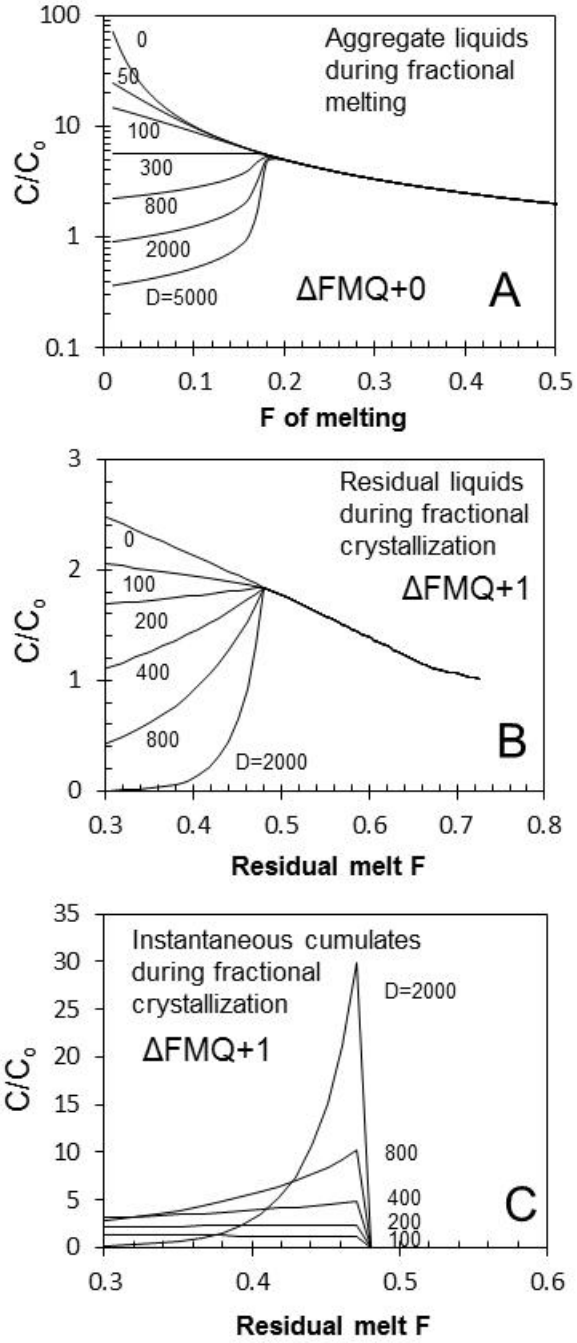

Fig. S2

These diagrams illustrate the effect of different sulfide partition coefficients on the behavior of chalcophile trace metals during melting and fractional crystallization. A) Concentration of an element in a melt as a function of degree of melting *F* for different sulfide partition coefficients D_{Sf}, assuming D for all other mineral phases is 0. If $D_{Sf} = 0$, then the element is controlled solely by silicate minerals, and if it is highly incompatible in silicates, it behaves as a perfectly incompatible element. If $D_{Sf}>>1$, then during early melting when sulfide is present, the element behaves as a compatible element and is thus

retained in the mantle residuum. Only when sulfide is exhausted from the mantle residuum does the element become incompatible. Melting calculations were done at FMQ+0. B) Composition of residual liquids as a function of fractionation degree (1-F, where F is the melt fraction). These calculations are done at FMQ+1, so the magma starts off under-saturated in S. Progressive fractionation of silicate minerals causes S content to increase in the residual magma because S behaves incompatibly. Thus, all chalcophile elements will also behave incompatibly. However, once sulfide-saturation is reached, sulfide precipitates. Strongly chalcophile elements (D_{Sf}>>1) will be efficiently stripped from the residual liquid, but elements with D_{Sf}=0 will remain incompatible and be enriched in the residual liquids. C) The complementary compositions of instantaneous cumulates during fractional crystallization. During initial fractional crystallization, the magma is assumed to be S-undersaturated, causing S and chalcophile elements to become enriched in the residual liquid. At S-saturation, sulfides precipitate as cumulates giving rise to cumulates with high abundances of chalcophile elements. Efficient enrichment in cumulates occurs for those elements with high D_{Sf}.

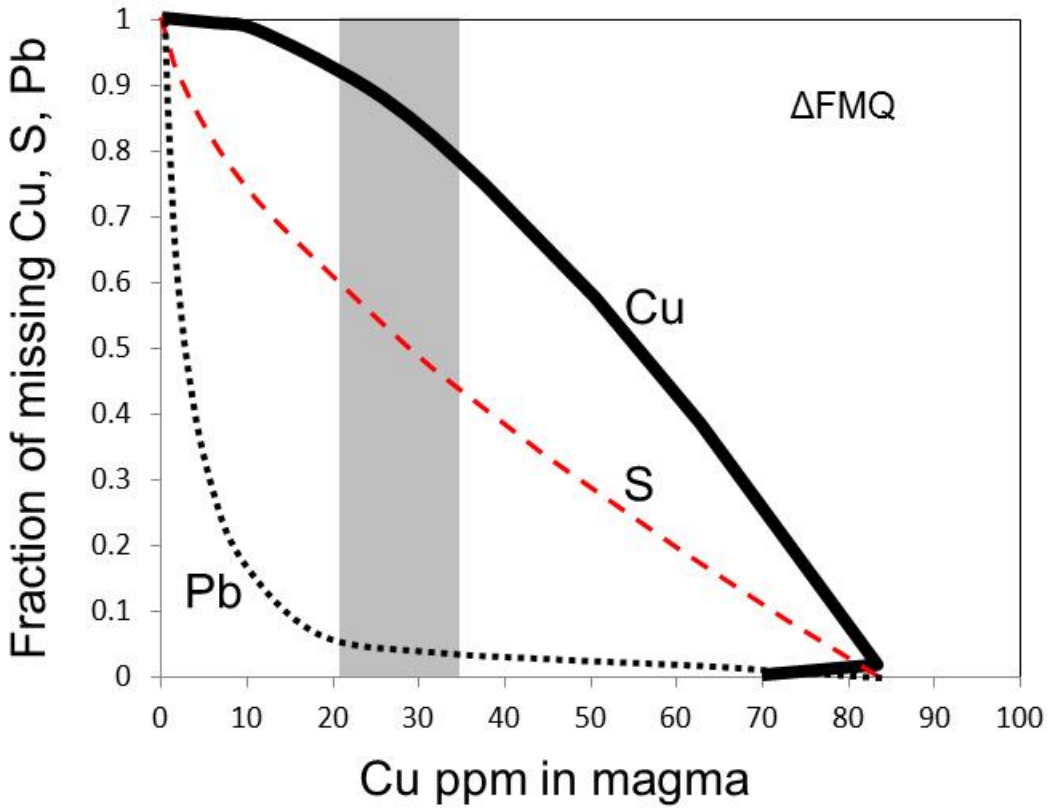

Fig. S3

Estimates of the amount of missing Cu, S and Pb in sulfide-bearing pyroxenites. Curves represent models of fractional crystallization as discussed above and in the main text. They show the fraction of missing Cu, S and Pb relative to the Cu content in the residual liquid. Gray vertical bar shows the Cu content of average continental crust and typical evolved arc magma. Intersection with the curves gives the amount of missing Cu, S and Pb.

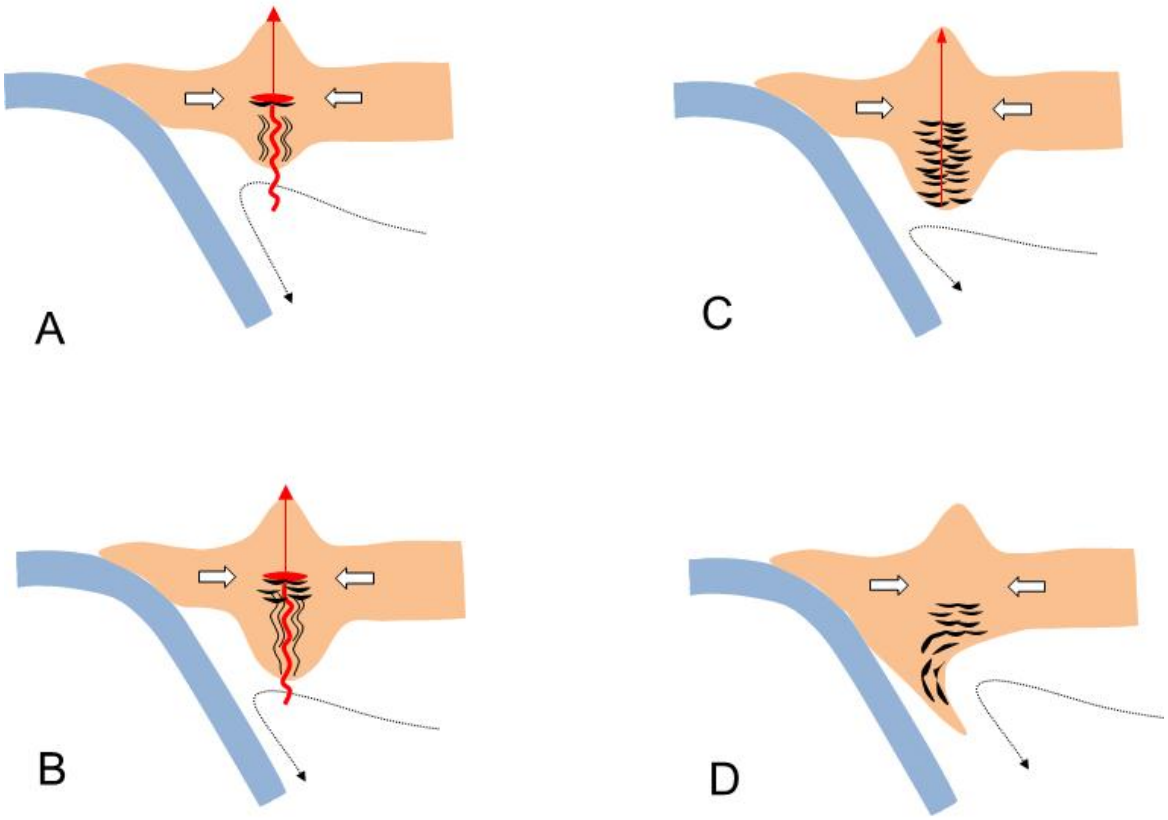

Fig. S4

Cartoon summarizing the Cu cycle during the evolution of an arc. A) Juvenile basaltic magmas (red arrow) transport Cu from the mantle wedge (open area) into the overlying arc lithosphere. Magmas undergo fractional crystallization to generate Cu-rich sulfide-bearing pyroxenites and amphibolites (black symbols). B) Thickening of the arc by magmatic inflation and lithospheric shortening (common in continental arcs), progressively forces fractionation to occur at greater depths, resulting in the development of a thick, sulfide-bearing pyroxenite (and amphibolite) root. C) As the root thickens, it becomes prone to re-melting. Because pyroxenites and amphibolites have low melting points compared to peridotitic mantle, they will undergo high-degree melting, generating Cu-rich felsic magmas that feed Cu-porphyries. D) If, however, the mafic root becomes gravitationally unstable before it melts, the sulfide-rich pyroxenite reservoir will be recycled back into the mantle.

References and Notes

1. R. J. Arculus, Oxidation status of the mantle: Past and present. *Annu. Rev. Earth Planet. Sci.* **13**, 75 (1985). doi:10.1146/annurev.ea.13.050185.000451

2. J. B. Gill, *Orogenic Andesites and Plate Tectonics* (Springer, Berlin, 1981).

3. I. S. E. Carmichael, The redox states of basic and silicic magmas: A reflection of their source regions? *Contrib. Mineral. Petrol.* **106**, 129 (1991). doi:10.1007/BF00306429

4. K. A. Kelley, E. Cottrell, Water and the oxidation state of subduction zone magmas. *Science* **325**, 605 (2009). doi:10.1126/science.1174156 Medline

5. J. E. Mungall, Roasting the mantle: Slab melting and the genesis of major Au and Au-rich Cu deposits. *Geology* **30**, 915 (2002). doi:10.1130/0091-7613(2002)030<0915:RTMSMA>2.0.CO;2

6. C.-T. A. Lee *et al*., The redox state of arc mantle using Zn/Fe systematics. *Nature* **468**, 681 (2010). doi:10.1038/nature09617 Medline

7. C.-T. A. Lee, W. P. Leeman, D. Canil, Z.-X. A. Li, Similar V/Sc systematics in MORB and arc basalts: Implications for the oxygen fugacities of their mantle source regions. *J. Petrol.* **46**, 2313 (2005). doi:10.1093/petrology/egi056

8. F. Jenner, H. S. C. O'Neill, R. J. Arculus, J. Mavrogenes, The magnetite crisis in the evolution of arc-related magmas and the initial concentration of Au, Ag and Cu. *J. Petrol.* **51**, 2445 (2010). doi:10.1093/petrology/egq063

9. N. Dauphas *et al*., Iron isotopes may reveal the redox conditions of mantle melting from Archean to present. *Earth Planet. Sci. Lett.* **288**, 255 (2009). doi:10.1016/j.epsl.2009.09.029

10. D. Canil, Vanadium partitioning and the oxidation state of Archaean komatiite magmas. *Nature* **389**, 842 (1997). doi:10.1038/39860

11. P. J. Jugo, Sulfur content at sulfide saturation in oxidized magmas. *Geology* **37**, 415 (2009). doi:10.1130/G25527A.1

12. P. J. Jugo, M. Wilke, R. E. Botcharnikov, Sulfur K-edge XANES analysis of natural and synthetic basaltic glasses: Implications for S speciation and S content as function of oxygen fugacity. *Geochim. Cosmochim. Acta* **74**, 5926 (2010). doi:10.1016/j.gca.2010.07.022

13. P. J. Wallace, Volatiles in subduction zone magmas: Concentrations and fluxes based on melt inclusion and volcanic gas data. *J. Volcanol. Geotherm. Res.* **140**, 217 (2005). doi:10.1016/j.jvolgeores.2004.07.023

14. E. M. Ripley, J. G. Brophy, C. Li, Copper solubility in a basaltic melt and sulfide liquid/silicate melt partition coefficients of Cu and Fe. *Geochim. Cosmochim. Acta* **66**, 2791 (2002). doi:10.1016/S0016-7037(02)00872-4

15. S. J. Lynton, P. A. Candela, P. M. Piccoli, An experimental study of the partitioning of copper between pyrrhotite and a high silica rhyolitic melt. *Econ. Geol.* **88**, 901 (1993). doi:10.2113/gsecongeo.88.4.901

16. G. A. Gaetani, T. L. Grove, Partitioning of moderately siderophile elements among olivine, silicate melt, and sulfide melt: Constraints on core formation in the Earth and Mars. *Geochim. Cosmochim. Acta* **61**, 1829 (1997). doi:10.1016/S0016-7037(97)00033-1

17. Materials and methods are available as supplementary material on *Science* Online

18. M. R. Handler, V. C. Bennett, G. Dreibus, Evidence from correlated Ir/Os and Cu/S for late-stage mobility in peridotite xenoliths: Implications for Re-Os systematics. *Geology* **27**, 75 (1999). doi:10.1130/0091-7613(1999)027<0075:EFCIOA>2.3.CO;2

19. W. F. McDonough, S.-S. Sun, The composition of the Earth. *Chem. Geol.* **120**, 223 (1995). doi:10.1016/0009-2541(94)00140-4

20. J.-P. Lorand, Abundance and distribution of Cu-Fe-Ni sulfides, sulfur, copper and platinum-group elements in orogenic-type spinel lherzolite massifs of Ariège (northeastern Pyrenees, France). *Earth Planet. Sci. Lett.* **93**, 50 (1989). doi:10.1016/0012-821X(89)90183-0

21. J. P. Lorand, Are spinel lherzolite xenoliths representative of the abundances of sulfur in the upper mantle? *Geochim. Cosmochim. Acta* **54**, 1487 (1990). doi:10.1016/0016-7037(90)90173-I

22. J. A. Mavrogenes, H. S. C. O'Neill, The relative effect of pressure, temperature and oxygen fugacity on the solubility of sulphide in mafic magmas. *Geochim. Cosmochim. Acta* **63**, 1173 (1999). doi:10.1016/S0016-7037(98)00289-0

23. H. S. C. O'Neill, J. A. Mavrogenes, The sulfide capacity and the sulfur content at sulfide saturation of silicate melts at 1400 °C and 1 bar. *J. Petrol.* **43**, 1049 (2002). doi:10.1093/petrology/43.6.1049

24. M. N. Ducea, Constraints on the bulk composition and root foundering rates of continental arcs: A California arc perspective. *J. Geophys. Res.* **107**, (B11), 2304 (2002). doi:10.1029/2001JB000643

25. M. N. Ducea, J. B. Saleeby, The age and origin of a thick mafic-ultramafic keel from beneath the Sierra Nevada batholith. *Contrib. Mineral. Petrol.* **133**, 169 (1998). doi:10.1007/s004100050445

26. C.-T. A. Lee, X. Cheng, U. Horodyskyj, The development and refinement of continental arcs by primary basaltic magmatism, garnet pyroxenite accumulation, basaltic recharge and delamination: Insights from the Sierra Nevada, California. *Contrib. Mineral. Petrol.* **151**, 222 (2006). doi:10.1007/s00410-005-0056-1

27. C.-T. A. Lee, D. M. Morton, R. W. Kistler, A. K. Baird, Petrology and tectonics of Phanerozoic continent formation: From island arcs to accretion and continental arc magmatism. *Earth Planet. Sci. Lett.* **263**, 370 (2007). doi:10.1016/j.epsl.2007.09.025

28. R. L. Rudnick, S. Gao, Composition of the continental crust. *Treatise Geochem.* **3**, 1 (2003). doi:10.1016/B0-08-043751-6/03016-4

29. J. Richards, Postsubduction porphyry Cu-Au and epithermal Au deposits: Products of remelting of subduction-modified lithosphere. *Geology* **37**, 247 (2009). doi:10.1130/G25451A.1

30. J. P. Richards, R. Kerrich, Adakite-like rocks: Their diverse origins and questionable role in metallogenesis. *Econ. Geol.* **102**, 537 (2007). doi:10.2113/gsecongeo.102.4.537

31. R. Oyarzun, A. Marquez, J. Lillo, I. Lopez, S. Rivera, Giant versus small porphyry copper deposits of Cenozoic age in northern Chile: Adakitic versus normal calc-alkaline magmatism. *Miner. Depos.* **36**, 794 (2001). doi:10.1007/s001260100205

32. R. Alonso-Perez, O. Müntener, P. Ulmer, Igneous garnet and amphibole fractionation in the roots of island arcs: Experimental constraints on andesitic liquids. *Contrib. Mineral. Petrol.* **157**, 541 (2009). doi:10.1007/s00410-008-0351-8

33. J. W. Hedenquist, J. B. Lowenstern, The role of magmas in the formation of hydrothermal ore deposits. *Nature* **370**, 519 (1994). doi:10.1038/370519a0

34. D. R. Cooke, P. Hollings, J. L. Walshe, Giant porphyry deposits: Characteristics, distribution, and tectonic controls. *Econ. Geol.* **100**, 801 (2005).

35. R. H. Sillitoe, Porphyry copper systems. *Econ. Geol.* **105**, 3 (2010). doi:10.2113/gsecongeo.105.1.3

36. M. Jull, P. Kelemen, On the conditions for lower crustal convective instability. *J. Geophys. Res.* **106**, (B4), 6423 (2001). doi:10.1029/2000JB900357

37. R. L. Rudnick, Making continental crust. *Nature* **378**, 571 (1995). doi:10.1038/378571a0

38. M. Haschke, J. Ahmadian, M. Murata, I. McDonald, Copper mineralization prevented by arc-root delamination during Alpine-Himalayan collision in central Iran. *Econ. Geol.* **105**, 855 (2010). doi:10.2113/gsecongeo.105.4.855

39. R. Arevalo, Jr., W. F. McDonough, Chemical variations and regional diversity observed in MORB. *Chem. Geol.* **271**, 70 (2010). doi:10.1016/j.chemgeo.2009.12.013

40. K. A. Kelley *et al*., Mantle melting as a function of water content beneath back-arc basins. *J. Geophys. Res.* **111**, (B9), B09208 (2006). doi:10.1029/2005JB003732 Medline

41. C.-T. A. Lee, D. M. Morton, R. W. Kistler, A. K. Baird, Petrology and tectonics of Phanerozoic continent formation: From island arcs to accretion and continental arc magmatism. *Earth Planet. Sci. Lett.* **263**, 370 (2007). doi:10.1016/j.epsl.2007.09.025

42. C.-T. A. Lee, X. Cheng, U. Horodyskyj, The development and refinement of continental arcs by primary basaltic magmatism, garnet pyroxenite accumulation, basaltic recharge and delamination: Insights from the Sierra Nevada, California. *Contrib. Mineral. Petrol.* **151**, 222 (2006). doi:10.1007/s00410-005-0056-1

43. U. Horodyskyj, C.-T. A. Lee, M. N. Ducea, Similarities between Archean high MgO eclogites and Phanerozoic arc-eclogite cumulates and the role of arcs in Archean continent formation. *Earth Planet. Sci. Lett.* **256**, 510 (2007). doi:10.1016/j.epsl.2007.02.006

44. M. N. Ducea, Constraints on the bulk composition and root foundering rates of continental arcs: A California arc perspective. *J. Geophys. Res.* **107**, (B11), 2304 (2002). doi:10.1029/2001JB000643

45. M. N. Ducea, J. B. Saleeby, Buoyancy sources for a large, unrooted mountain range, the Sierra Nevada, California: Evidence from xenolith thermobarometry. *J. Geophys. Res.* **101**, (B4), 8229 (1996). doi:10.1029/95JB03452

46. M. N. Ducea, J. B. Saleeby, The age and origin of a thick mafic-ultramafic keel from beneath the Sierra Nevada batholith. *Contrib. Mineral. Petrol.* **133**, 169 (1998). doi:10.1007/s004100050445

47. C.-T. A. Lee *et al*., The redox state of arc mantle using Zn/Fe systematics. *Nature* **468**, 681 (2010). doi:10.1038/nature09617 Medline

48. Z.-X. A. Li, C.-T. A. Lee, Geochemical investigation of serpentinized oceanic lithospheric mantle in the Feather River Ophiolite, California: Implications for the recycling rate of water by subduction. *Chem. Geol.* **235**, 161 (2006). doi:10.1016/j.chemgeo.2006.06.011

49. C.-T. A. Lee, M. Oka, P. Luffi, A. Agranier, Internal distribution of Li and B in serpentinites from the Feather River Ophiolite, California based on laser ablation inductively coupled plasma mass spectrometry. *Geochem. Geophys. Geosyst.* **9**, (2009). 10.1029/2008GC002078

50. S. Gao *et al*., Determination of forty two major and trace elements in USGS and NIST SRM glasses by laser ablation-inductively coupled plasma-mass spectrometery. *Geostand. Newsl.* **26**, 181 (2002). doi:10.1111/j.1751-908X.2002.tb00886.x

51. A. J. Campbell, M. Humayun, M. K. Weisberg, Siderophile element constraints on the formation of metal in the metal-rich chondrites Bencubbin, Weatherford, and Gujba. *Geochim. Cosmochim. Acta* **66**, 647 (2002). doi:10.1016/S0016-7037(01)00794-3

52. V. Le Roux, R. Dasgupta, C.-T. A. Lee, Mineralogical heterogeneities in the Earth's mantle: Constraints from Mn, Co, Ni and Zn partitioning during partial melting. *Earth Planet. Sci. Lett.* **307**, 395 (2011). doi:10.1016/j.epsl.2011.05.014

53. V. Le Roux, C.-T. A. Lee, S. J. Turner, Zn/Fe systematics in mafic and ultramafic systems: Implications for detecting major element heterogeneities in the Earth's mantle. *Geochim. Cosmochim. Acta* **74**, 2779 (2010). doi:10.1016/j.gca.2010.02.004

54. C.-T. A. Lee, A. Harbert, W. P. Leeman, Extension of lattice strain theory to mineral/mineral rare-earth element partitioning: An approach for assessing disequilibrium and developing internally consistent partition coefficients between olivine, orthopyroxene, clinopyroxene, and basaltic melt. *Geochim. Cosmochim. Acta* **71**, 481 (2007). doi:10.1016/j.gca.2006.09.014

55. E. H. Hauri, T. P. Wagner, T. L. Grove, Experimental and natural partitioning of Th, U, Pb and other trace elements between garnet, clinopyroxene and basaltic melts. *Chem. Geol.* **117**, 149 (1994). doi:10.1016/0009-2541(94)90126-0

56. G. Mallmann, H. S. C. O'Neill, The crystal/melt partitioning of V during mantle melting as a function of oxygen fugacity compared with some other elements (Al, P, Ca, Sc, Ti, Cr, Fe, Ga, Y, Zr and Nb). *J. Petrol.* **50**, 1765 (2009). doi:10.1093/petrology/egp053

57. E. Takahashi, Melting of a dry peridotite KLB-1 up to 14 GPa: Implications on the origin of peridotitic upper mantle. *J. Geophys. Res.* **91**, (B9), 9367 (1986). doi:10.1029/JB091iB09p09367

58. M. J. Walter, Melting of garnet peridotite and the origin of komatiite and depleted lithosphere. *J. Petrol.* **39**, 29 (1998). doi:10.1093/petrology/39.1.29

59. W. L. Griffin, D. R. Cousens, C. G. Ryan, G. F. Suter, Ni in chrome pyrope garnets: A new geothermometer. *Contrib. Mineral. Petrol.* **103**, 199 (1989). doi:10.1007/BF00378505

60. J. A. Mavrogenes, H. S. C. O'Neill, The relative effect of pressure, temperature and oxygen fugacity on the solubility of sulphide in mafic magmas. *Geochim. Cosmochim. Acta* **63**, 1173 (1999). doi:10.1016/S0016-7037(98)00289-0

61. H. S. C. O'Neill, J. A. Mavrogenes, The sulfide capacity and the sulfur content at sulfide saturation of silicate melts at 1400 °C and 1 bar. *J. Petrol.* **43**, 1049 (2002). doi:10.1093/petrology/43.6.1049

62. P. J. Jugo, M. Wilke, R. E. Botcharnikov, Sulfur K-edge XANES analysis of natural and synthetic basaltic glasses: implications for S speciation and S content as function of oxygen fugacity. *Geochim. Cosmochim. Acta* **74**, 5926 (2010). doi:10.1016/j.gca.2010.07.022

63. E. M. Ripley, J. G. Brophy, C. Li, Copper solubility in a basaltic melt and sulfide liquid/silicate melt partition coefficients of Cu and Fe. *Geochim. Cosmochim. Acta* **66**, 2791 (2002). doi:10.1016/S0016-7037(02)00872-4

64. T. Sugawara, Empirical relatioships between temperature, pressure, and MgO content in olivine and pyroxene saturated liquid. *J. Geophys. Res.* **105**, (B4), 8457 (2000). doi:10.1029/2000JB900010

65. S. R. Hart, G. A. Gaetani, Mantle Pb paradoxes: The sulfide solution. *Contrib. Mineral. Petrol.* **152**, 295 (2006). doi:10.1007/s00410-006-0108-1

66. R. L. Rudnick, S. Gao, Composition of the continental crust. *Treatise Geochem.* **3**, 1 (2003). doi:10.1016/B0-08-043751-6/03016-4

67. B. H. Wilkinson, S. E. Kesler, Quantitative identification of metallogenic epochs and provinces: Application to Phanerozoic porphyry copper deposits. *Econ. Geol.* **104**, 607 (2009). doi:10.2113/gsecongeo.104.5.607